2011 American Control Conference
on O'Farrell Street, San Francisco, CA, USA
June 29 - July 01, 2011

Optimal power system unit commitment with guaranteed local stability

Wolfgang Grote and Darya Kastsian and Martin Mönnigmann.

Abstract— **This article deals with the cost optimal commitment of power systems. System stability is often only considered after solving the commitment problem. We show by example that a cost optimization may result in a mode of operation that, while economically optimal, is unstable or has otherwise unacceptable dynamics. As a remedy, we propose to use the so-called normal vector method, which has been developed for the optimization of nonlinear dynamical systems with stability boundaries and uncertain parameters. We apply the method to a small sample power grid, where the optimization goal is to minimize the energy production costs for a given power consumption.**

I. INTRODUCTION

Cost-optimization of power system operation is usually performed without consideration of stability of the underlying dynamical system [1], [2]. On the other hand it is well-known that power plants stability and grid stability are not trivial [3], [4], [5]. We present an optimization method based on nonlinear programming and bifurcation theory that takes stability boundaries into account during the optimization process. The method, which is usually referred to as the normal vector method, has originally been developed for the steady state optimization of continuous-time nonlinear dynamical systems with stability boundaries and uncertain parameters [6], [7]. It has recently been extended to the steady state optimization of discrete-time systems and the certain types of transient optimizations of continuous-time systems [8]. In the present paper the method is used to state stability constraints in mixed-integer (or mixed-logic) nonlinear programs for the first time to the knowledge of the authors. Formally, the system class reads

$$\dot{x} = f(x, \alpha, s), \tag{1}$$

where $x \in \mathbb{R}^{n_x}$, $\alpha \in \mathbb{R}^{n_\alpha}$, and $s \in \{0,1\}$ denote state variables, system parameters, and logic variables, respectively. Furthermore, f is assumed to be sufficiently smooth.

The paper is organized as follows. In Sect. II we introduce the small sample grid and the optimization task. Section III explains the normal vector method, which is applied to the sample grid in Sect. IV. Conclusions are given in Sect. V.

II. DYNAMIC MODEL OF A SIMPLE SAMPLE POWER SYSTEM

Consider the simple grid shown in Fig. 1, which is adopted from [9]. The sample island grid consists of three power plants and three power consumers that are connected in a ring structure. Power plant 1 is fueled by coal, plant 2 is a river hydro station, and plant 3 is driven by a gas turbine. All power plants can be deenergized in the model by opening the respective grid breaker s_i. Whenever the grid breaker s_i is opened, power plant i does not contribute to the operating cost of the grid. Power is assumed to be distributed symmetrically to the three phases, which implies that the grid can be reduced to a one wire representation. Transmission lines are modeled as constant impedances $(z_4, \ldots, z_9)$. The three loads are also modeled by impedances (z_a, z_b, z_c) that represent the apparent power S of the current consumption. Two scenarios with different loads are examined. These scenarios are summarized in Tab. III in the appendix. Transformer and

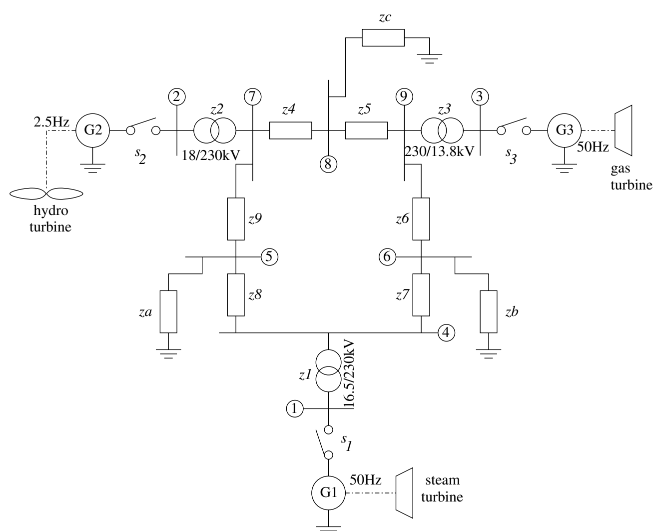

Fig. 1. Circuit diagram of the sample grid

generator reactances of each generator node are represented by impedances z_1, z_2, and z_3. The optimization task is to minimize the energy production cost. We assume a proportional relationship between the mechanical shaft power and the energy production cost of each power plant. Taking the grid breaker positions s_i, $i = 1, \ldots, 3$ into account, the cost function reads

$$C(P_0, s) = \sum_i s_i \cdot c_i \cdot P_{0i} \quad \text{in } \frac{\text{EUR}}{\text{h}}. \tag{2}$$

We note that a more elaborate cost function would have to take load-dependent efficiencies and fuel-independent costs into account. Here we prefer a simple cost function, however, because it results in a more transparent exposition of the proposed robust optimization method. The costs coefficients $c_1 = 33\,\frac{\text{EUR}}{\text{MWh}}$, $c_2 = 15\,\frac{\text{EUR}}{\text{MWh}}$, and $c_3 = 108\,\frac{\text{EUR}}{\text{MWh}}$ are adopted from [10].

Automatic Control and Systems Theory, Ruhr-Universität Bochum, Universitätsstr. 150, 44801 Bochum, Germany, Email: grote@rus.rub.de, darya.kastsian@rub.de, martin.moennigmann@rub.de

The dynamic model of the grid is based on the equilibrium of electrical active power and the mechanical shaft power of each generator, where the classic equations of motion are applied [9], [11], [12]. The model equations read

$$\frac{\mathrm{d}x_i}{\mathrm{d}t} = x_{3+i} - s_i\omega_0, \tag{3a}$$

$$\frac{\mathrm{d}x_{3+i}}{\mathrm{d}t} = \frac{S_n}{\Theta_i \cdot x_{3+i}}\left[P_{mi} - P_{ei}\right], \tag{3b}$$

where index i=1,…,3, x_1, x_2, x_3 are the rotor angles of the generators, x_4, x_5, x_6 are the angular velocities of the rotors, ω_0 is the nominal grid frequency, Θ_i is the inertia of the i-th drive shaft, P_{mi} is the i-th mechanical turbine power, and P_{ei} is the active power of the i-th generator. If damping of the damper windings is to be taken into account, each of the last three equations in (3) must be extended by a damping power term $P_{di}(x_4, x_5, x_6)$. The electrical active powers can be calculated from

$$P_{ei} = |u_i|^2 \cdot \Re(Y^\star_{ii}(s)) + \sum_{k=1,\ k\neq i}^{n_g} |u_i| \cdot |u_k| \cdot \Big[\Im(Y^\star_{ik}(s)) \cdot \sin(x_i - x_k) + \Re(Y^\star_{ik}(s)) \cdot \cos(x_i - x_k)\Big], \tag{4}$$

where u_i denotes the generator node voltages, n_g is the number of generators (here $n_g = 3$), and $Y^\star_{ik}$ denotes the i-th row and the k-th column of the reduced grid admittance matrix $Y^\star$ of the grid shown in Fig. 1. The matrix $Y^\star$ is defined in Eq. (5) below. It depends on the state of the switches $s = (s_1, s_2, s_3)^T$, $s_i \in \{0,1\}$.

For the case with three switches treated here, there exist $2^3 = 8$ different admittance matrices. Note that the number of admittance matrices grows exponentially in the number of switches. The admittance matrix of the grid, which depends on s, reads

$$Y(s) = \left[\begin{array}{ccc|cccccc}
s_1y_1 & 0 & 0 & -s_1y_1 & 0 & 0 & 0 & 0 & 0 \\
0 & s_2y_2 & 0 & 0 & 0 & 0 & -s_2y_2 & 0 & 0 \\
0 & 0 & s_3y_3 & 0 & 0 & 0 & 0 & 0 & -s_3y_3 \\
\hline
-s_1y_1 & 0 & 0 & s_1y_1+y_7+y_8 & -y_8 & -y_7 & 0 & 0 & 0 \\
0 & 0 & 0 & -y_8 & y_8+y_9+y_a & 0 & -y_9 & 0 & 0 \\
0 & 0 & 0 & -y_7 & 0 & y_6+y_7+y_b & 0 & 0 & -y_6 \\
0 & -s_2y_2 & 0 & 0 & -y_9 & 0 & s_2y_2+y_4+y_9 & -y_4 & 0 \\
0 & 0 & 0 & 0 & 0 & 0 & -y_4 & y_4+y_5+y_c & -y_5 \\
0 & 0 & -s_3y_3 & 0 & 0 & -y_6 & 0 & -y_5 & s_3y_3+y_5+y_6
\end{array}\right] = \begin{bmatrix} Y_{11} & Y_{12} \\ Y_{21} & Y_{22} \end{bmatrix},$$

where the block matrix stated in the last equations is introduced for ease of reference. Admittances $y_j = 1/z_j$, where $j \in \{1,\dots,9\} \cup \{a,b,c\}$, can be obtained from the impedances z_j given in Tab. III. The dynamic model uses an admittance matrix

$$Y^\star = Y_{11} - Y_{12}Y_{22}^{-1}Y_{21} \tag{5}$$

that is reduced to the generator nodes. The effect of the grid breakers s_i on the grid admittances is illustrated by two examples. If all breakers are closed, i.e. $s = (1,1,1)$, the reduced admittance matrix for load case 1 reads

$$Y^\star = \begin{bmatrix} 0.2875-2.991j & 0.4533+1.471j & 0.3286+0.967j \\ 0.4533+1.471j & 0.9691-4.226j & 0.6869+1.658j \\ 0.3286+0.967j & 0.6869+1.658j & 0.6607-3.499j \end{bmatrix}.$$

In contrast, $Y^\star = \mathrm{diag}(1.4396-2.5652j, 0, 0)$ if only the coal power plant is delivering energy.

The grid must include a frequency controller for stabilization. We assume that frequency control is performed by one of the power plants. We do not choose this power plant a priori, however, but the task of frequency control is assigned to one of the plants by the optimization problem. Frequency control is achieved by delivering more or less energy by increasing respectively decreasing the mechanical shaft power P_{mi}:

$$P_{mi} = P_{0i} + \underbrace{\left[K_R(\omega_0 - \omega_i) + K_I \int (\omega_0 - \omega_i)\mathrm{d}t\right]}_{\text{controller equation (PI)}} \cdot s_{ci}, \tag{6}$$

where the rotor speed is denoted by $\omega_i = x_{n_g+i}$, the proportional controller gain is K_R and the integral controller gain is K_I.

We introduce a Boolean variable $s_{ci} \in \{0,1\}$ to model the choice of the frequency controller, where $s_{ci} = 1$ and $s_{cj} = 0$ for $j \neq i$, if the frequency control is assigned to the i-th power plant. Specifically, we choose the values stated in Tab. I, which are assumed to be given by the network operator. Table I can equivalently be stated as the logic constraints

TABLE I

CHOICE OF THE SPEED CONTROLLING POWER PLANT

s_1	s_2	s_3	s_{c1}	s_{c2}	s_{c3}
0	0	0	0	0	0
0	0	1	0	0	1
0	1	0	0	1	0
0	1	1	0	1	0

s_1	s_2	s_3	s_{c1}	s_{c2}	s_{c3}
1	0	0	1	0	0
1	0	1	0	0	1
1	1	0	0	1	0
1	1	1	0	1	0

$$s_{c1} = s_1\bar{s}_2\bar{s}_3, \quad s_{c2} = s_2, \quad s_{c3} = \bar{s}_2 s_3. \tag{7}$$

Two optimization scenarios are considered that differ with respect to the power consumption. In the first scenario the consumption is so high that all power plants are forced to be run to satisfy the demands. In the second scenario less power is consumed. Therefore, there exists the possibility to provide the power by the operation of only two of the three power plants. The power consumption is stated in Tab. II for the two scenarios.

The optimization task amounts to finding an energy mix P_{0i}, $i = 1,2,3$, that results in minimum electricity production costs. Since the Boolean variables s_i, $i = 1,2,3$, are free variables of the optimization, the optimization algorithm may choose to deenergize some power plants by setting some s_i to zero. Stability and robustness are enforced in the optimization as explained in the subsequent section.

III. STEADY STATE OPTIMIZATION WITH CONSTRAINTS FOR ROBUST LOCAL ASYMPTOTIC STABILITY

This section introduces the so-called normal vector method and normal vector constraints. These constraints can, among other applications, be used to enforce local asymptotic stability of optimal solutions of nonlinear steady state optimization problems. Moreover, the normal vector constraints ensure robustness in the sense that the optimized nonlinear system remains locally asymptotically stable in a finite (non-local) vicinity of the optimal point. This second property of the method can conveniently be used in the optimization of systems with uncertain design or operating parameters as detailed below. Originally, the normal vector method has been developed for the systems with continuous parameters [6], [7], [8], [13]. In the present paper the normal vector method is applied to a dynamical system with Boolean variables ($s_i \in \{0,1\}$) for the first time to the knowledge of the authors.

We introduce the proposed method for robust optimization in three steps for ease of presentation: (1) optimization *without* normal vector constraints and *fixed* grid structure, (2) optimization *with* normal vector constraints and *fixed* grid structure, and (3) optimization *with* normal vector constraints and *free* grid structure. In cases (1) and (2) the grid structure is fixed by preassigning the values of $s_i \in \{0,1\}$, $i = 1,2,3$. In case (3), in contrast, the s_i are subject to optimization and thus are chosen by the optimization algorithm. We stress that steps (1) and (2) are only introduced to simplify the exposition of case (3), which is the problem type we are actually interested in.

a) Optimization without normal vector constraints and fixed grid structure: Assume that the positions of the switches shown in Fig. 1 are fixed. For example, all switches s_i may be closed to enforce operation of all plants, i.e. $s = (1,1,1)^T$. In such a case, optimizing the steady state operating cost of the grid amounts to solving a constrained nonlinear program (NLP) of the form

$$\min_{P_0^{(0)}} \quad C(P_0^{(0)}, s)$$

$$\text{s.t.} \quad 0 = f(x^{(0)}, P_0^{(0)}, s), \tag{8a}$$

$$0 \leq P_{i,max} - P_{0i}^{(0)} \text{ for } i = 1,2,3, \tag{8b}$$

$$0 = \sum_{i=1}^{3} P_{0i}^{(0)} - \sum_{i=a,b,c} \Re(y_i), \tag{8c}$$

where $C(P_m^{(0)}, s)$ is the cost function (2). The set of equations (8a) restricts solutions to steady states of model (3). Note that the frequency control for $s = (1,1,1)^T$ is performed by the hydro power plant and $s_c = (0,1,0)^T$ is substituted in (6). Constraints (8b) bound P_{0i}, $i = 1,2,3$ from above. The last constraint (8c) ensures that the total generated power equals the total consumed power.

It is well-known that naively solving the NLP (8) may result in a steady state that is cost optimal but unstable [6]. The normal vector constraints introduced in the next section can be used to restrict the optimization to stable steady states.

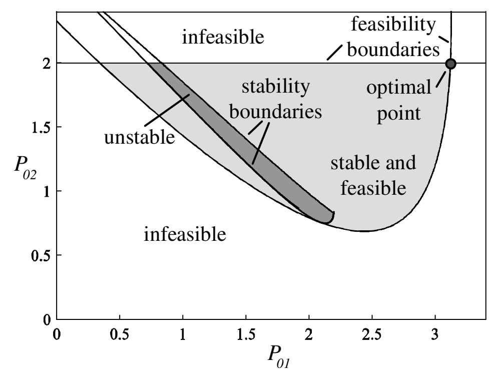

Fig. 2. Critical boundaries of system (3) where $s = (1,1,1)^T$. Powers are given in per unit values, where 1 unit = 100 MW. The optimal point is discussed in Sect. IV.

b) Optimization with normal vector constraints and fixed grid structure: In order to ensure the stability of the optimal solution $(x^{(0)}, P_0^{(0)}, s)$ of the NLP (8), additional constraints are necessary that guarantee the real parts of all eigenvalues λ_j of the Jacobian $f_x(x^{(0)}, P_0^{(0)}, s)$ to be negative. Since finding explicit expressions for eigenvalues λ_j of the Jacobian of a nonlinear system is tedious if not impossible, we use implicit constraints that are based on ideas from applied bifurcation theory. Due to their geometric interpretation discussed below, these constraints are referred to as normal vector constraints [6] (see [14] for the original idea of the normal vector to bifurcation boundaries).

Figure 2 shows critical boundaries in the parameter space (P_{01}, P_{02}) for the system (3) for $s = (1,1,1)^T$. Two feasibility boundaries and one stability boundary are shown that separate feasible from infeasible and stable from unstable regions, respectively. The linear feasibility boundary results from the constraint on the maximal size of the hydro turbine $P_{02} \leq$ 200 MW (see Tab. IV). The nonlinear feasibility boundary originates form the upper bound on the difference in rotor angles (90°) of the generators. The region that results due to the existence of feasibility and stability boundaries is shaded in Fig. 2. Critical boundaries like those in Fig. 2 can be obtained, for example, with the freely available MATLAB toolbox MATCONT [15]. The results obtained from this toolbox can be also used for initialization of the optimal problems discussed below.

We are interested in identifying the optimal steady state of operation in the desired stable and feasible region. Beyond guaranteeing stability of the optimal point we ensure robustness by, loosely speaking, putting a safety region around the optimal point. This is illustrated in Fig. 3. The square in Fig. 3 corresponds to the robustness region

$$P_{0i}^{(0)} \in [P_{0i}^{(0)} - \Delta P_{0i}, P_{0i}^{(0)} + \Delta P_{0i}] \quad \text{for } i = \{1,2\}, \tag{9}$$

or equivalently,

$$\frac{P_{0i}^{(0)}}{\Delta P_{0i}} \in [\frac{P_{0i}^{(0)}}{\Delta P_{0i}} - 1, \frac{P_{0i}^{(0)}}{\Delta P_{0i}} + 1] \quad \text{for } i = \{1,2\}, \tag{10}$$

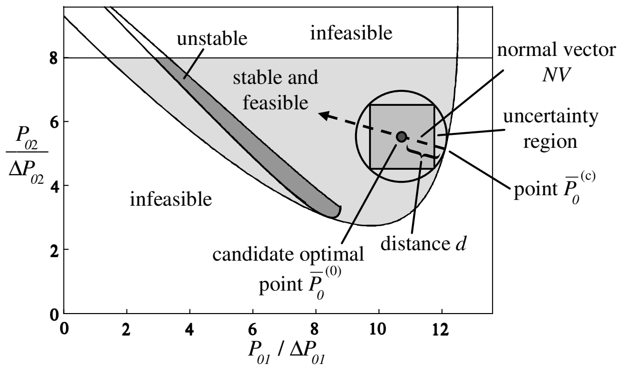

Fig. 3. Critical boundaries of system (3) where $s = (1,1,1)^T$ in the scaled parameter space ($\Delta P_{01} = \Delta P_{02} = 0.25$).

where the scaled parameters $\bar{P}_{0i}^{(0)} := P_{0i}^{(0)}/\Delta P_{0i}$ and $\bar{P}_{0i}^{(c)} := P_{0i}^{(c)}/\Delta P_{0i}$ are introduced merely for convenience. The essential idea of the normal vector method is to force this robustness region into the feasible and stable area as sketched in Fig. 3. In doing so we guarantee that there exists a locally asymptotically stable steady state of the nonlinear system for any value of P_{0i}, $i = 1,2$ within the robustness region. In this sense stability can be guaranteed, even though some or all system parameters are uncertain.

The constraint for robust stability sketched in Fig. 3 can be stated formally by imposing the additional constraints

$$\bar{P}_0^{(0)} = \bar{P}_0^{(c)} + d\frac{NV}{\|NV\|}, \quad d \geq d_{min}, \tag{11}$$

where $\|\cdot\|$ denotes Euclidean norm and the normal vector NV defines the ray that passes through the candidate optimal point and that is normal to the closest point on the critical (stability or feasibility) boundary. In Fig. 3 the value of d_{min} must be set to

$$d_{min} = r_{rob} := \sqrt{2}, \tag{12}$$

where r_{rob} denotes the radius of the circle which encloses the uncertainty box (10) of side length 2. While the idea of the normal vector constraint is illustrated in two dimensions, it applies to the general case of n_α uncertain parameters. In this case Eq. (10) is replaced by an n_α-dimensional hypersquare that is enclosed by an n_α-dimensional ball of radius $r_{rob} = \sqrt{n_\alpha}$.

Augmenting the NLP (8) by the normal vector constraints results in the following NLP, in which we still assume s to be fixed.

$$\begin{aligned}
\min_{P_0^{(0)}} \quad & C(P_0^{(0)}, s) \\
\text{s.t.} \quad & \text{Constraints (8a) – (8c)}, && (13a)\\
& 0 = G_k(\bar{x}_k^{(c)}, \tilde{x}_k^{(c)}, \bar{P}_{0,k}^{(c)}, NV_k, s) \quad \forall k \in K, && (13b)\\
& 0 = \bar{P}_{0,k}^{(c)} - \bar{P}_0^{(0)} + d_k\frac{NV_k}{\|NV_k\|} \quad \forall k \in K, && (13c)\\
& 0 \leq d_k - r_{rob} \quad \forall k \in K. && (13d)
\end{aligned}$$

The first part of NLP (13) is the same as NLP (8). The set of equations (13b) describes the critical boundary $k \in K$ and its normal vector NV_k to it, where we assume that K such critical boundaries have to be taken into account. Furthermore, $\tilde{x}_k$ denotes auxiliary variables, and $\bar{P}_{0,k}^{(c)}$ is the point on the critical boundary k that is connected to the candidate optimal point $\bar{P}_0$. For the full mathematical representation and derivation of set G_k we refer the reader to [6]. The last two constraints(13c) and (13d) assure that the resulting optimal point is far enough from the critical boundary k, i.e. distance d_k is larger or equal to radius $r_{rob} = \sqrt{2}$. If this inequality constraints becomes active, i.e. $d_k = r_{rob}$, the circle around the uncertainty region touches the critical boundary k. This situation is shown in Fig. 3.

We stress that the location of the critical boundaries need not be known before solving the NLP (13), but can be detected automatically [7].

c) Optimization with normal vector constraints and free grid structure: Finally, we assume that the structure of the grid is not known a priori, i.e., the s_i are no longer fixed, but become optimization variables. Consequently, the NLPs (8) and (13) become nonlinear programs with integer, or binary, variables. The NLP (8) is replaced by

$$\begin{aligned}
\min_{P_0^{(0)}, s^{(0)}} \quad & C(P_0^{(0)}, s^{(0)}) \\
\text{s.t.} \quad & 0 = f(x^{(0)}, P_0^{(0)}, s^{(0)}), && (14a)\\
& \text{Logic constraints (7)}, && (14b)\\
& 0 \leq P_{i,max} - P_{0i}^{(0)} \text{ for } i = 1,2,3, && (14c)\\
& 0 = \sum_{i=1}^{3} P_{0i}^{(0)} - \sum_{i=a,b,c} \Re(y_i), && (14d)
\end{aligned}$$

Similarly, the NLP (13) is replaced by

$$\begin{aligned}
\min_{P_0^{(0)}, s^{(0)}} \quad & C(P_0^{(0)}, s^{(0)}) \\
\text{s.t.} \quad & \text{Constraints (14a) – (14d)}, && (15a)\\
& 0 = G_k(\bar{x}_k^{(c)}, \tilde{x}_k^{(c)}, \bar{P}_{0,k}^{(c)}, NV_k, s^{(0)}) \ \forall k \in K, && (15b)\\
& 0 = \bar{P}_{0,k}^{(c)} - \bar{P}_0^{(0)} + d_k\frac{NV_k}{\|NV_k\|} \quad \forall k \in K, && (15c)\\
& 0 \leq d_k - r_{rob} \quad \forall k \in K. && (15d)
\end{aligned}$$

We solve problems of the form (14) and (15) with the commercial solver SBB in GAMS [16].

IV. ROBUST OPTIMIZATION

In this section we optimize the two scenarios introduced in Sect. II by applying the method from Sect. III. The goal is to find optimal steady states that are stable and robust by solving problems of the form (15) with normal vector constraints. We also solve optimization problems *without* normal vector constraints of the form (14), however. The latter results are calculated for reference. In particular, these reference results show that the normal vector constraints are necessary as will become clear further below.

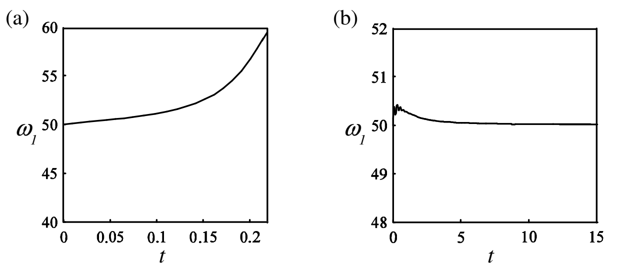

Fig. 4. Step responses of the steam turbine frequency $\omega_1 = x_4/(2\pi)$ after an increase in P_{01} by 10% for the optimal points obtained without (a) and with (b) normal vector method with free grid structure for the first scenario.

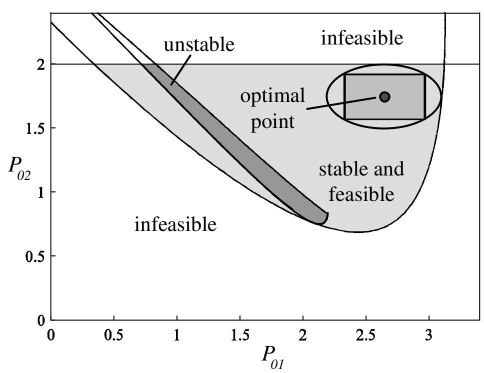

Fig. 5. Optimal point obtained with the normal vector constraints and free grid structure for the first scenario.

d) Optimization of scenario 1: Figure 2 shows the optimal point that results from solving (15), i.e. the optimization without constraints on dynamics and free grid structure. At this optimal point all switches are closed ($s = (1,1,1)^T$). The plants are running at

$$P_{01}^{(0)} = 312\,\mathrm{MW}, P_{02}^{(0)} = 200\,\mathrm{MW}, P_{03}^{(0)} = 90\,\mathrm{MW}, \qquad (16)$$

and the cost function (2) evaluates to $230.16\,\frac{\mathrm{EUR}}{\mathrm{MWh}}$ at this point. Figure 2 shows that the optimal point (16) is critically feasible, since it lies on the intersection of two feasibility boundaries. Any increase of P_{01} or P_{02} into the infeasible region therefore results in a loss of synchronization. If the power delivered by the turbine of $G1$ is increased by 10%, for example, no steady state of operation exists anymore. This is illustrated in Fig. 4 (a). Clearly, the departure from $\omega_1 = 50\,\mathrm{Hz}$ shown in this figure is inacceptable and must be avoided to guarantee stable plant and grid operation.

In the remainder of this section we use the normal vector method to find a robust optimal point. We assume that P_{0i}, $i = 1,2$ may vary by 10% around the reference values (18) and require all steady states that may result within this uncertainty to be feasible and locally asymptotically stable. Specifically, we solve the optimization problem (15) with normal vector constraints to both feasibility boundaries depicted in Fig. 2 and the uncertainties $\Delta P_{01} = 31.2\,\mathrm{MW}$ and $\Delta P_{02} = 20\,\mathrm{MW}$. Figure 5 shows the resulting optimal point which corresponds to the grid structure $s = (1,1,1)^T$

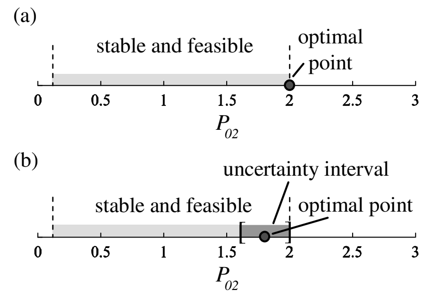

Fig. 6. Optimal point obtained without (top Fig. (a)) and with (bottom Fig. (b)) normal vector method with free grid structure for the second scenario.

with generated powers $P_{01}^{(0)} = 266\,\mathrm{MW}$, $P_{02}^{(0)} = 172\,\mathrm{MW}$, and $P_{03}^{(0)} = 164\,\mathrm{MW}$. The cost function (2) evaluates to $290.7\,\frac{\mathrm{EUR}}{\mathrm{MWh}}$ at this point. This value is about 25% larger than the cost at the critically feasible point (16). Essentially, this increase in cost is the price to be paid for robust operation.

Figure 4 (b) illustrates the robustness of the optimal point obtained with the normal vector constraints. In contrast to the unacceptable behavior shown in Fig. 4 (a), the step response remains well below 1 Hz deviation for the robust optimal point.

e) Optimization of scenario 2: For the second scenario we proceed in the same way as for scenario 1. The optimization without constraints on the dynamics, which is again carried out for reference, results in an optimal point of operation that is not robust. More precisely, solving the optimization problem (14) without constraints on dynamics and free grid structure results in the optimal point $s = (1,1,0)^T$ with

$$P_{01}^{(0)} = 107\,\mathrm{MW}, P_{02}^{(0)} = 200\,\mathrm{MW}, \qquad (17)$$

4 where the cost function evaluates to $65.31\,\frac{\mathrm{EUR}}{\mathrm{MWh}}$. As opposed to the result for scenario 1 switch s_3 is open in this case, thus the gas turbine is not operating ($P_{03}^{(0)} = 0\,\mathrm{MW}$).

The optimal point (17) is illustrated in Fig. 6 (a). Since only two plants are present, and since the sum of generated powers is fixed, a one-dimensional figure results. P_{01} can be calculated from $P_{01}^{(0)} = 307\,\mathrm{MW} - P_{02}^{(0)} - P_{03}^{(0)}$, where $P_{03}^{(0)} = 0\,\mathrm{MW}$. Just as for scenario 1 the optimal point is stable but critically feasible in that P_{02} attains a value on the boundary of the feasible region $14\,\mathrm{MW} \leq P_{02} \leq 200\,\mathrm{MW}$.

In order to find a robust optimal point we optimize the scenario with normal vector constraints. The robustness region is the trivial interval $[P_{02}^{(0)} - \Delta P_{02}, P_{02}^{(0)} + \Delta P_{02}]$ in this case. Just as in scenario 1 we set ΔP_{02} to 10% of its value at the reference optimal point obtained without normal vectors (17), which gives $\Delta P_{02} = 20\,\mathrm{MW}$. In this trivial case with only one uncertain parameter, the normal vector distance constraint (11) reads

$$\bar{P}_{02}^{(0)} = \bar{P}_{02}^{(c)} - d, \quad d \geq 1, \qquad (18)$$

which is equivalent to the simple linear constraint $P_{02}^{(0)} \leq P_{02}^{(c)} - \Delta P_{02}$, i.e. $P_{02}^{(0)} \leq 180\,\mathrm{MW}$.

Figure 6 (b) shows the result of the optimization with the normal vector constraints (18). The optimal point is given by $P_{01}^{(0)} = 127\,\mathrm{MW}$, $P_{02}^{(0)} = 180\,\mathrm{MW}$, $P_{03}^{(0)} = 0\,\mathrm{MW}$, $s^{(0)} = (1,1,0)^T$, and the cost function (2) equals $68.91\,\frac{\mathrm{EUR}}{\mathrm{MWh}}$. As compared to the result obtained without constraints on dynamics (17) the cost increased by about 5%. Just as in the first scenario, this increase can be interpreted as the cost of robustness.

V. CONCLUSIONS

We considered the cost optimal commitment of power plants within a given power grid. A simple grid of three plants and three consumers served an illustrative example throughout the paper. We demonstrated for this example that the so-called normal vector method can be used to guarantee steady state stability of operation in the search for an optimal point of operation. Moreover, we demonstrated that parametric uncertainty can be addressed systematically with the normal vector method. Stability and robustness constraints proved useful when solving the cost optimal commitment problem, since a naive optimization resulted in unstable points of operation for the grid, or points of operation with otherwise unacceptable dynamical properties. Having given a proof of concept, the method will be applied to the commitment problem in more realistic grids in the future.

VI. ACKNOWLEDGMENTS

The project this work is based on was funded by E.ON AG as part of the E.ON Research Initiative. Responsibility for the content of this publications lies with the authors.

APPENDIX

TABLE II

ACTIVE AND REACTIVE POWER CONSUMPTION OF THE 2 SCENARIOS

First scenario			
P_a	192 MW	Q_a	+38 MVAR
P_b	162 MW	Q_b	+27 MVAR
P_c	248 MW	Q_c	+25 MVAR
P_Σ	602 MW	Q_Σ	90 MVAR
Second scenario			
P_a	99 MW	Q_a	+10 MVAR
P_b	83 MW	Q_b	+7 MVAR
P_c	125 MW	Q_c	+6 MVAR
P_Σ	307 MW	Q_Σ	23 MVAR

TABLE III

IMPEDANCES z_j OF THE GRID FOR THE 2 SCENARIOS

Imp. z_j	p.u.	Imp. z_j	p.u.
z_1	0.20j	First scenario	
z_2	0.05j	z_a	0.50 + 0.10j
z_3	0.10j	z_b	0.60 + 0.10j
z_4	0.25j	z_c	0.40 + 0.04j
z_5	0.16j	Second scenario	
z_6	0.17j	z_a	1.00 + 0.10j
z_7	0.09j	z_b	1.20 + 0.10j
z_8	0.09j	z_c	0.80 + 0.04j
z_9	0.12j		

TABLE IV

PARAMETERS OF THE POWER SYSTEM MODEL

Symbol	Meaning	Value	Unit
K_I	integral gain (speed contr.)	0.05	-
K_R	proport. gain (speed contr.)	0.10	-
n_g	number of synchr. generators	0.10	-
$P_{1,max}$	max. output power of PP 1	350	MW
$P_{2,max}$	max. output power of PP 2	200	MW
$P_{3,max}$	max. output power of PP 3	200	MW
S_n	app. power for p.u.-norm	100	MVA
u_n	grid voltage	230	kV
Θ_1	inertia of rotor 1	10,000	$\mathrm{kg\,m^2}$
Θ_2	inertia of rotor 2	4,000	$\mathrm{kg\,m^2}$
Θ_3	inertia of rotor 3	6,000	$\mathrm{kg\,m^2}$
ω_0	nominal angular grid freq.	$2\pi \cdot 50$	$\frac{1}{s}$
ω_i	ang. frequency of PP-rotor #i	$2\pi \cdot f_i$	$\frac{1}{s}$

REFERENCES

[1] J. Momoh, *Electric Power System Applications of Optimization*. CRC Press, 2001.

[2] J. Zhu, *Optimization of Power System Operation (IEEE Press Series on Power Engineering)*. Hoboken, NJ: Wiley-IEEE Press, 2009.

[3] E. Vittal, M. O'Malley, and A. Keane, "A steady-state voltage stability analysis of power systems with high penetrations of wind," *IEEE Transactions on Power Systems*, vol. 25, no. 1, pp. 433–42, February 2010.

[4] Z. Dong, Y. Makarov, and D. Hill, "Genetic algorithms in power system small signal stability analysis," 1997, pp. 342–347, 4th International Conference on Advances in Power System Control, Operation & Management, Wanchai, Hong Kong.

[5] X. Lei, E. Lerch, and D. Povh, "Unit commitment at frequency security condition," *European Transactions on Electrical Power*, vol. 11, no. 2, pp. 89–96, 2001.

[6] M. Mönnigmann and W. Marquardt, "Normal vectors on manifolds of critical points for parametric robustness of equilibrium solutions of ODE systems," *J. Nonlinear Sci.*, vol. 12, no. 2, pp. 85–112, 2002.

[7] M. Mönnigmann, W. Marquardt, C. H. Bischof, T. Beelitz, B. Lang, and P. Willems, "A hybrid approach for efficient robust design of dynamic systems," *SIAM Rev.*, vol. 49, no. 2, pp. 236–254, 2007.

[8] J. Gerhard, W. Marquardt, and M. Mönnigmann, "Normal vectors on critical manifolds for robust design of transient processes in the presence of fast disturbances," *SIAM J. Appl. Dyn. Syst.*, vol. 7, no. 2, pp. 461–490, 2008.

[9] P. Anderson and A. Fouad, *Power System Control and Stability (IEEE Press Series on Power Engineering)*. Hoboken, NJ: Wiley-IEEE Press, 2003.

[10] P. Konstantin, *Praxisbuch Energiewirtschaft*. Berlin: Springer, 2007.

[11] P. Kundur, *Power System Stability and Control*. New York: McGraw-Hill, 1994.

[12] D. Nelles, *Netzdynamik*. Berlin: VDE, 2009.

[13] D. Kastsian and M. Mönnigmann, "Robust optimization of fixed points of nonlinear discrete time systems with uncertain parameters," *SIAM J. Appl. Dyn. Syst.*, vol. 9, pp. 357–390, 2010.

[14] I. Dobson, "Computing a closest bifurcation instability in multidimensional parameter space," *J. Nonlinear Sci.*, vol. 3, no. 3, pp. 307–327, 1993.

[15] A. Dhooge, W. Govaerts, and Y. A. Kuznetsov, "MATCONT: A MATLAB package for numerical bifurcation analysis of ODEs," *ACM Trans. Math. Softw.*, vol. 29, no. 2, pp. 141–164, 2003.

[16] *Solver Manual of SBB*, ARKI Consulting and Development A/S, http://www.gams.com/solvers/solvers.htm, 2002.

[17] E. Welfonder, Ed., *Regelungs- und Optimierungskonzepte für den koordinierten Kraftwerks- und Netzbetrieb*, VDI/VDE-Gesellschaft Mess- und Automatisierungstechnik. Düsseldorf: VDI Verlag, 1996.

[18] C. Canizares, "Calculating optimal system parameters to maximize the distance to saddle-node bifurcations," *IEEE Transactions on Circuits and Systems I - Regular Papers*, vol. 45, no. 3, pp. 225–237, 1998.